Application of FE-BECM in Field Analysis of Induction Coil Gun

Shoubao Liu, Jiangjun Ruan, Yadong Zhang, Yu Zhang, and Yujiao Zhang

***Abstract*—This paper builds a field model of induction coil gun based on finite-element and boundary-element coupling method (FE-BECM). The fundamental of FE-BECM is introduced, and it is used in open-boundary eddy-current problem to prove its validity and find a way to reduce a nonconforming error. In the coil gun's FE-BECM model, the coil and projectile are discretized by finite elements; boundary elements are used to discretize the free space and associate unconnected finite-element regions. In FE-BECM model, the coordinates of nodes that belong to moving bodies change when movement occurs. The distribution of magnetic flux density and eddy current during the launch process is displayed. The result of FE-BECM is compared with experimental data and results of other numerical methods.**

***Index Terms*—Eddy current, finite-element and boundary-element coupling method (FE-BECM), induction coil gun, movement.**

I. Introduction

COIL GUN is an importance member in electromagnetic launch (EML) family [1]. In the analysis of coil gun, circuit method was widely used. In circuit method, the projectile is equivalent to a set of concentric conductive rings; all the excitation coils and conductive rings are replaced by RLC circuits. The electrical and mechanical equations governing the behaviors of the system are formulated on the basis of the adopted equivalent network [2].

The launch process of EML is a complex electromagnetic transient; the circuit model cannot provide information of field distribution during launch. In order to realize electromagnetic optimization design, more and more attention is paid to field simulation [3].

The field calculation of EML is a problem of eddy-current field involving movement. With the introduction of movement, one of the main problems encountered in the numerical analysis is the management of grid according to the relative movement of components in system [4]. The method of remeshing is adopted in finite-element software ANSOFT, and a 2-D coil gun example is reported in [5]. The technique of sliding meshes is adopted in MEGA; its application in coil gun field simulation is introduced in [6]. The use of composite grid method (CGM) in coil gun's field simulation can be found in [4] and [7].

Manuscript received January 6, 2010; revised April 9, 2010; accepted May 16, 2010. Date of publication July 15, 2010; date of current version January 7, 2011.

S. Liu, J. Ruan, Y. Zhang, and Yj. Zhang are with the School of Electrical Engineering, Wuhan University, Wuhan 430072, China.

Y. Zhang is with Jiangxi Provincial Electric Power Company, Nanchang 330077, China.

Color versions of one or more of the figures in this paper are available online at http://ieeexplore.ieee.org.

Digital Object Identifier 10.1109/TPS.2010.2051164

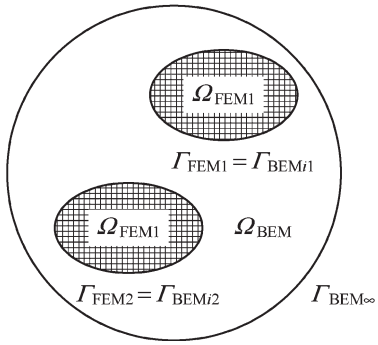

Fig. 1. Structure of solution region.

In this paper, finite-element and boundary-element coupling method (FE-BECM) is used to build 3-D model of a single-stage coil gun. In the model, two unconnected regions which contain excitation coil and projectile, respectively, are meshed by finite elements; boundary elements exist on the surface of the two regions to discretize the free space and associate the two sets of finite elements. When the projectile moves, it only needs to change the coordinates of nodes in the moving region. Thus, the trouble of remeshing in conventional finite-element method (FEM) based on one set of grid is overcome. Compared with sliding meshes, FE-BECM is able to deal with problems that contain arbitrary movement; compared with CGM, FE-BECM is more suitable for parallel computation [8] and more convenient to operate.

II. Fundamentals of FE-BECM

A. Discrete Region and Boundary Condition

The discrete region of FE-BECM is shown in Fig. 1, the considered region is $\Omega = \Omega_{\mathrm{FEM1}} \cup \Omega_{\mathrm{FEM2}} \cup \Omega_{\mathrm{BEM}}$, and boundary elements exist on surface $\Gamma_{\mathrm{BEM}} = \Gamma_{\mathrm{BEM}i1} \cup \Gamma_{\mathrm{BEM}i2} \cup \Gamma_{\mathrm{BEM}\infty}$.

Finite elements of different regions do not have topological constraint; boundary elements that exist on the surface of FEM regions discretize free space and associate FEM regions.

On interface between free space and FEM regions, the boundary condition can be expressed [9]

$$\boldsymbol{A}^{\mathrm{FEM}} = \boldsymbol{A}^{\mathrm{BEM}} \tag{1}$$

$$\nabla \cdot \boldsymbol{A}^{\mathrm{FEM}} = \nabla \cdot \boldsymbol{A}^{\mathrm{BEM}} \tag{2}$$

$$\nu \nabla \times \boldsymbol{A} \times \boldsymbol{n}\big|^{\mathrm{FEM}} = -\nu \nabla \times \boldsymbol{A} \times \boldsymbol{n}\big|^{\mathrm{BEM}} \Leftrightarrow \boldsymbol{H}_t^{\mathrm{FEM}} = -\boldsymbol{H}_t^{\mathrm{BEM}} \tag{3}$$

where ν denotes reluctivity, $\boldsymbol{n}$ denotes the normal vector of surface of FEM region, and the subscript t in (3) denotes

tangent direction. The minus signs in (3) are due to the change of orientation of $\boldsymbol{n}$ on the interface.

B. Finite-Element Formulation

The regions Ω_{FEMi} which contain source and eddy currents is discretized by finite element; the governing equations in those regions can be written as

$$\nabla \times \nu \nabla \times \boldsymbol{A} + \sigma \left(\nabla \phi + \frac{\partial \boldsymbol{A}}{\partial t} \right) = \boldsymbol{J} \tag{4}$$

$$\nabla \cdot \sigma \left(\nabla \phi + \frac{\partial \boldsymbol{A}}{\partial t} \right) = 0 \tag{5}$$

where σ denotes conductivity. In finite-element region Ω_{FEMj}, the Galerkin method yields the weak integral formulation of (4) and (5) as follows [10]:

$$\int_{\Omega_j} \nu(\nabla \times N_i) \cdot (\nabla \times \boldsymbol{A}) d\Omega - \int_{\Gamma_j} \nu \nabla \times \boldsymbol{A} \times \boldsymbol{n} \cdot N_i d\Gamma + \int_{\Omega_j} \sigma \left(\nabla \phi + \frac{\partial \boldsymbol{A}}{\partial t} \right) \cdot N_i d\Omega = \int_{\Omega_j} \boldsymbol{J} \cdot N_i \mathrm{d}\Omega \tag{6}$$

$$\int_{\Omega_j} \sigma \left(\nabla \phi + \frac{\partial \boldsymbol{A}}{\partial t} \right) \cdot \nabla N_i d\Omega = 0. \tag{7}$$

In (6) and (7), N_i is the shape function of element Ω_j, and Γ_j is the interface of FEM and BEM regions. The second term on the left side of (6) can be expressed as

$$\nu \nabla \times \boldsymbol{A} \times \boldsymbol{n} = \boldsymbol{H}_t. \tag{8}$$

By combining (6) and (7), the global stiffness matrix of FEM reads

$$\boldsymbol{K}\{\boldsymbol{A}^{\mathrm{FEM}}, \phi^{\mathrm{FEM}}\} - \boldsymbol{T}\boldsymbol{H}_t^{\mathrm{FEM}} = \boldsymbol{F} \tag{9}$$

where $\boldsymbol{K}$ is a stiff matrix of FEM and $\boldsymbol{T}$ is the boundary matrix.

C. Boundary-Element Formulation

Boundary elements discretize free space; the governing equation in free space is written as

$$\nabla^2 \boldsymbol{A} = 0. \tag{10}$$

By a set of integral transforms of (10), the direct BEM integral equation is expressed as [11]

$$\int_{\Omega_{\mathrm{BEM}}} \boldsymbol{A} \nabla^2 u^* d\Omega + \int_{\Gamma_{\mathrm{BEM}}} u^* \boldsymbol{Q} d\Gamma - \int_{\Gamma_{\mathrm{BEM}}} q^* \boldsymbol{A} d\Gamma = 0 \tag{11}$$

with

$$\boldsymbol{Q} = (\boldsymbol{n} \cdot \nabla)\boldsymbol{A} \tag{12}$$

$$u^* = 1/4\pi r \tag{13}$$

$$q^* = \frac{\partial u^*}{\partial n} \tag{14}$$

where r is the distance between source and field points. Since the boundary elements only exist on the interface of regions, the volume integral in (11) is canceled. Thus, we get

$$c_i \boldsymbol{A} + \int_{\Gamma_{\mathrm{BEM}}} q^* \boldsymbol{A} d\Gamma = \int_{\Gamma_{\mathrm{BEM}}} \boldsymbol{u}^* \boldsymbol{Q} d\Gamma. \tag{15}$$

Express (15) in a discrete form; thus, the boundary element can be written as

$$\boldsymbol{H}\boldsymbol{A}^{\mathrm{BEM}} = \boldsymbol{G}\boldsymbol{Q}^{\mathrm{BEM}}. \tag{16}$$

D. Equivalent Finite-Element Matrix

Combining boundary conditions (2) and (3), one gets [12]

$$(\boldsymbol{n} \mathrm{g} \nabla)\boldsymbol{A}^{\mathrm{FEM}} = -(\boldsymbol{n} \mathrm{g} \nabla)\boldsymbol{A}^{\mathrm{BEM}} \Leftrightarrow \boldsymbol{Q}^{\mathrm{FEM}} = -\boldsymbol{Q}^{\mathrm{BEM}}. \tag{17}$$

Therefore, (9) can now be written as

$$\boldsymbol{K}\{\boldsymbol{A}^{\mathrm{FEM}}, \phi^{\mathrm{FEM}}\} - \boldsymbol{T}\boldsymbol{Q}^{\mathrm{FEM}} = \boldsymbol{F}. \tag{18}$$

Because of the boundary conditions (1) and (17), (16) and (18) can be combined, and we can get the final equations of FE-BECM in equivalent finite-element matrix

$$(\boldsymbol{K} + \boldsymbol{K}_{\mathrm{BEM}})\{\boldsymbol{A}^{\mathrm{FEM}}, \phi^{\mathrm{FEM}}\} = \boldsymbol{F} \tag{19}$$

where

$$\boldsymbol{K}_{\mathrm{BEM}} = \boldsymbol{T}\boldsymbol{G}^{-1}\boldsymbol{H}. \tag{20}$$

Equation (19) is the discrete equation for open-boundary eddy-current problem with $\boldsymbol{A} = 0$ at $\Gamma_{\mathrm{BEM}\infty}$, and the domain Ω_{BEM} has been mapped onto an equivalent FEM matrix $\boldsymbol{K}_{\mathrm{BEM}}$.

III. Nonconforming Error of FE-BECM

When the BEM grids are located on the surface of different materials, a nonconforming error will be introduced. It is because field changes sharply on the interface of different materials [4], [7]. A method to reduce such error is to extend the region of FEM to include a layer of meshes with the same material as the BEM grids.

To explore modeling principle and prove the validity of FE-BECM, models of TEAM workshop problem number 7 (TEAM 7) were built. The description of TEAM 7 can be found in [13]. According to the form of air layer, three different FE-BECM models were built.

A. Without Air Layer

In this case, the boundary elements are located on the surface of entities. The coil, aluminum plate, and air block that wraps observation line are meshed by eight-nodal hexahedral elements. The interfaces are meshed by quadrilateral elements. The discretization of that model is shown in Fig. 2.

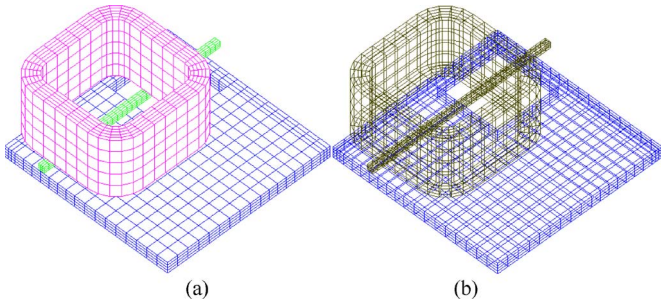

Fig. 2. Discretization of FE-BECM model without air layer. (a) FEM elements. (b) Perspective of BEM elements.

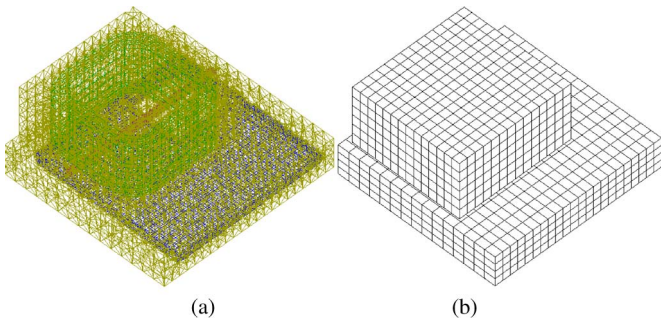

Fig. 3. Discretization of FE-BECM model with two air layers. (a) Perspective of finite elements. (b) Boundary elements.

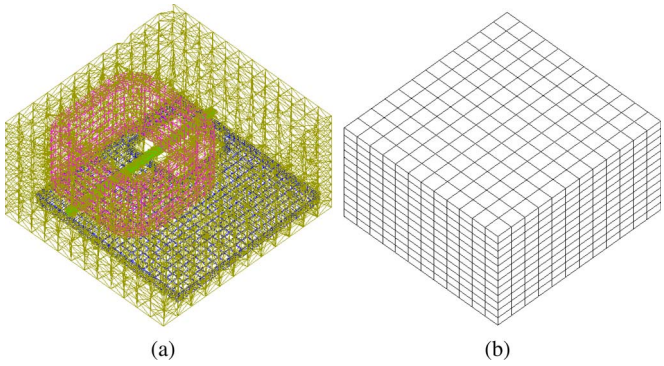

Fig. 4. Discretization of FE-BECM model with a whole air layer. (a) Perspective of FEM elements. (b) BEM elements.

B. With Two Air Layers

In this model, the coil and aluminum plate are wrapped with air blocks, respectively. The air layers are discretized by four-nodal tetrahedral elements, as shown in Fig. 3.

C. With a Whole Air Layer

In this model, the coil and aluminum plate are wrapped by a whole air block (as shown in Fig. 4).

Field distribution of the model is show in Fig. 5.

The discretization information of those FE-BECM models is listed in Table I.

A comparison of results of the FE-BECM models with measurement of flux density's real part on the observation line is shown in Fig. 6.

From Table I and Fig. 6, we can see that the existence of air layer has a great influence on the results. In the model wrapped by a whole air layer, the simulation result achieves good agreement with the measurement result. With the enlargement of air layer, the numbers of BEM elements and nodes decrease but the calculation precision is improved. Thus, it is reasonable to use an air layer and properly enlarge its spatial scope when building the FE-BECM model to reduce the nonconforming error in dealing with the open-boundary eddy-current problem.

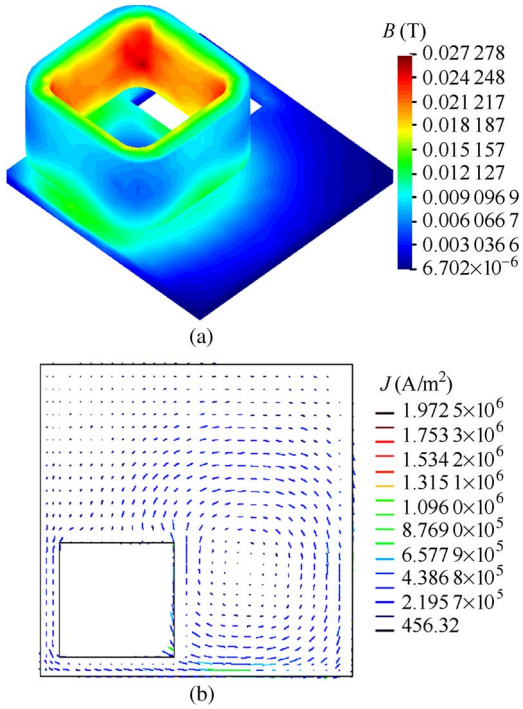

Fig. 5. Field distribution of FE-BECM model with a whole air layer. (a) Contour of real part of flux density. (b) Vectogram of real part of eddy current.

TABLE I
DISCRETIZATION INFORMATION OF THE THREE FE-BECM MODELS

Model	FEM elements	FEM nodes	BEM elements	BEM nodes
Without air layer	2 572	3 852	2 290	2 292
With two air layers	41 551	14 856	1 460	1 464
With a whole air layer	58 621	16 200	864	866

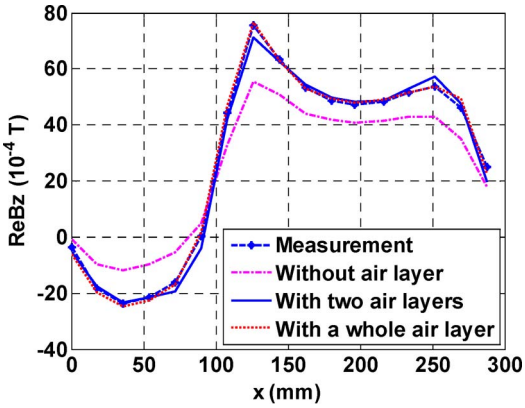

Fig. 6. Results of FE-BECM models and measure.

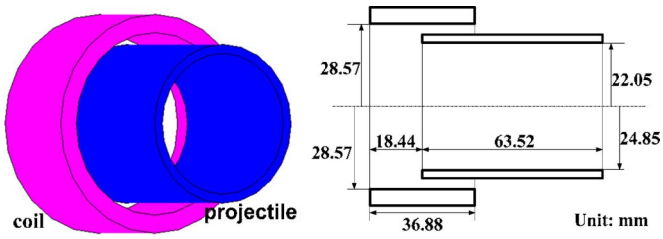

Fig. 7. Schematic drawing of single-stage coil gun and dimensions.

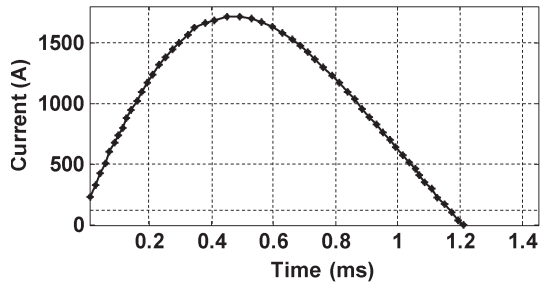

Fig. 8. Waveform of excitation current.

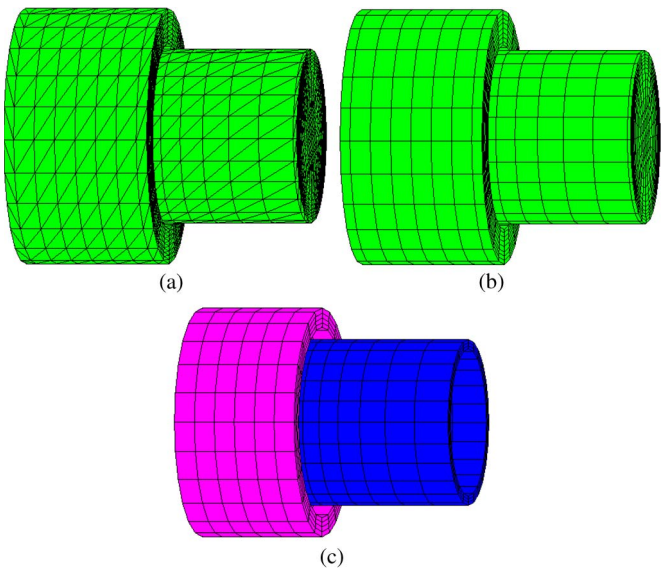

Fig. 9. (a) BEM elements on the surface, (b) FEM elements in air layers, and (c) FEM element in coil and projective.

IV. Analysis of Coil Gun Model

This section analyzes the electromagnetic transient of single-stage coil gun by FE-BECM. The model (as shown in Fig. 7) is from [6], where the experimental data and result of 2-D sliding meshes are available.

The projectile of the coil gun model is an aluminum cylinder (3E7 S/m). The coil has 60 turns. The waveform of excitation current is shown in Fig. 8.

According to the analysis result of Section III, two air layers are used to wrap excitation coil and projectile, respectively. The surface of the two air layers is discretized by triangular BEM elements; excitation coil, projectile, and air regions are discretized by hexahedral FEM elements (shown in Fig. 9).

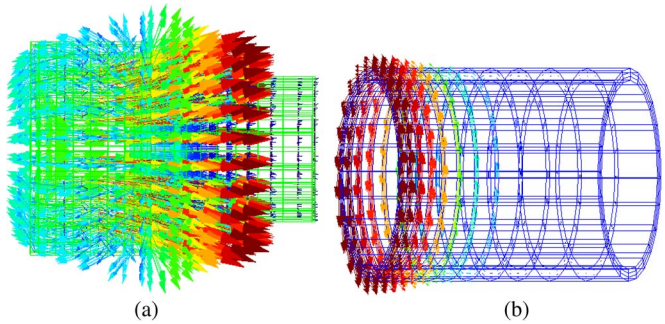

Fig. 10. (a) Flux density and (b) eddy-current distribution at 0.45 ms.

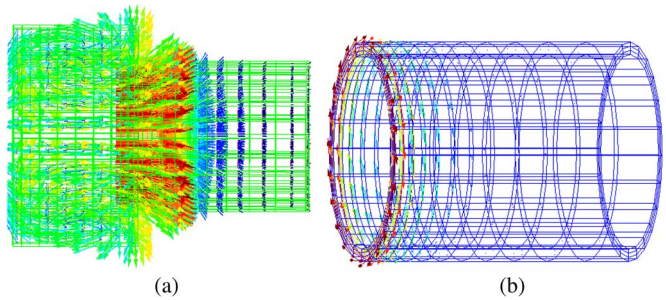

Fig. 11. (a) Flux density and (b) eddy-current distribution at 0.9 ms.

In every time step, we calculate the flux distribution and electromagnetic force $\boldsymbol{F}$ on projectile, and $\boldsymbol{F}$ is calculated by a virtual work method [14]. Then, the movement of projectile is realized by changing the coordinates of nodes in the moving region, which include the projectile and the air layer that wrapped it.

By $\boldsymbol{F}$ and the mass of projectile, we can get the projectile's acceleration a, and then, the velocity and location of projectile can be obtained by following equations:

$$\nu_{n+1} = \nu_n + a\Delta t \tag{21}$$

$$x_{n+1} = x_n + (\nu_n + \nu_{n+1})\Delta t/2 \tag{22}$$

where ν_n and ν_{n+1} are the projectile's velocity of the current and succeeding times, respectively, in meters per second; x_n and x_{n+1} is the projectile's location (in meters) in the direction of muzzle at the current and succeeding times; and Δt is the time step in seconds.

The Euler backward difference [15] is used in time discretization. The value of Δt is 0.03 ms; the initial velocity of projectile is 0 m/s. In every time, step flux density, eddy-current density, and electromagnetic force are calculated. By (21) and (22), the velocity and position of projectile at the succeeding time are obtained. Then, the coordinates of nodes in the moving region are changed, and the calculation of the succeeding time starts.

Field distributions at 0.45 and 0.9 ms are shown in Figs. 10 and 11.

From Figs. 10 and 11, we can see that the maximum magnetic flux density always appears at the rear part of the projectile, which is a traveling magnetic field produced by excitation coils moving ahead with the projectile. The induced eddy current mainly distributes in the rear part of the projectile. At the two

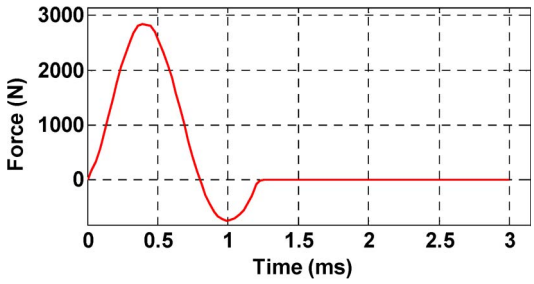

Fig. 12. Force waveform of projectile.

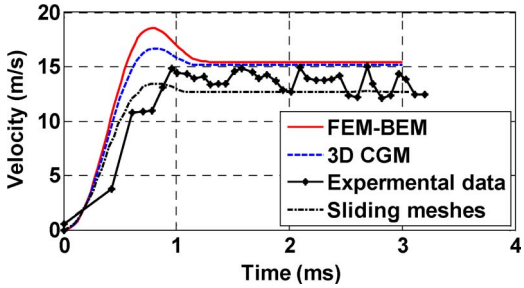

Fig. 13. Velocity results of FE-BECM, 3-D CGM, sliding meshes, and experimental data.

different times, the axial component of eddy current changes direction; since the direction of excitation current is unchanged, the direction of flux density produced by the coil is unchanged, thus leading to the change of the direction of $\boldsymbol{F}$. The waveform of $\boldsymbol{F}$ is shown in Fig. 12.

From Fig. 12, we can see that the projectile was accelerated by the Lorentz force in most time of the launch; since the eddy current in the rear part of the projectile changes direction in the last part, the force changed direction, and the projectile was retarded.

The projectile's velocity calculated by FE-BECM is shown in Fig. 13, in which the results obtained from 3-D CGM in [4], 2-D sliding meshes, and experimental data in [6] are also displayed. It can be seen from Fig. 13 that the velocity result of FE-BECM is in reasonable agreement with the experimental data and the results of other numerical methods.

V. Conclusion

The fundamental of FE-BECM has been introduced, and the nonconforming error of FE-BECM has been analyzed. The single-stage coil gun's 3-D FE-BECM model is built, and the field distribution during launch is obtained. By comparing with the results of other numerical method and experimental data, the validity of FE-BECM has been proved.

Since the multistage coil gun gets more and more attention, FE-BECM should be applied in field analysis of more complex case. In the field model, the current of excitation coil is not known in advance; in order to complete the whole analysis process and predict the electromagnetic performance of the coil gun system, FE-BECM should be combined with the coil gun's existing circuit methods to build the coil gun's field-circuit model.

References

[1] W. Ying, R. A. Marshall, and C. Shukang, *Physics of Electric Launch*. Beijing, China: Science Press, 2004, pp. 136–150.

[2] J. He, E. Levi, Z. Zabar, and L. Birenbaum, "Concerning the design of capacitively driven induction coil guns," *IEEE Trans. Magn.*, vol. 17, no. 3, pp. 429–438, Jun. 1989.

[3] S. Liu, J. Ruan, and D. Huang, "Analysis of inductive coil gun performance based on field coupling circuit method," in *Proc. IEEE 6th Int. Power Electron. Motion Control Conf.*, Wuhan, China, 2009, pp. 845–849.

[4] Z. Yu, R. Jiangjun, G. Yan, P. Ying, and D. Zhiye, "Application of a composite grid method in the analysis of 3-D eddy current field involving movement," *IEEE Trans. Magn.*, vol. 44, no. 6, pp. 1298–1301, Jun. 2008.

[5] K. Zhao, S. Cheng, and R. Zhang, "Influence of driving current's wave on accelerative performance of induction coil launcher," in *Proc. 14th Symp. Electromagn. Launch Technol.*, Victoria, BC, Canada, 2008, pp. 1–4.

[6] P. J. Leonard, H. C. Lai, G. Hainsworth, D. Rodger, and J. F. Eastham, "Analysis of the performance of tubular pulsed coil induction launchers," *IEEE Trans. Magn.*, vol. 29, no. 1, pp. 686–690, Jan. 1993.

[7] P. Ying, R. Jiangjun, Z. Yu, and G. Yan, "A composite grid method for moving conductor eddy-current problem," *IEEE Trans. Magn.*, vol. 43, no. 7, pp. 3259–3265, Jul. 2007.

[8] V. Rischmuller, M. Haas, S. Kurz, and W. M. Rucker, "3D transient analysis of electromechanical devices using parallel BEM coupled to FEM," *IEEE Trans. Magn.*, vol. 36, no. 4, pp. 1360–1363, Jul. 2000.

[9] S. Kurz, J. Fetzer, and G. Lehner, "An improved algorithm for the BEM-FEM-coupling method using domain decomposition," *IEEE Trans. Magn.*, vol. 31, no. 1, pp. 1727–1740, May 1995.

[10] O. Biro and K. Preis, "On the use of the magnetic vector potential in the finite-element analysis of three-dimensional eddy currents," *IEEE Trans. Magn.*, vol. 25, no. 4, pp. 3145–3159, Jul. 1989.

[11] J. Fetzer, S. Kurz, and G. Lehner, "Comparison of analytical and numerical integration techniques for the boundary integrals in the BEM–FEM coupling considering TEAM workshop problem no. 13," *IEEE Trans. Magn.*, vol. 33, no. 2, pp. 1227–1230, Mar. 1997.

[12] S. Kurz, J. Fetzer, and G. Lehner, "Three dimensional transient BEM–FEM coupled analysis of electrodynamic levitation problems," *IEEE Trans. Magn.*, vol. 32, no. 3, pp. 1062–1065, May 1996.

[13] H. Tsuboi, M. Tanaka, K. Ikeda, and K. Nishimura, "Computation results of the TEAM workshop problem 7 by finite element methods using tetrahedral and hexahedral elements," *J. Mater. Process. Technol.*, vol. 108, no. 2, pp. 237–240, Jan. 4, 2001.

[14] A. Benhama, A. C. Williamson, and A. B. J. Reece, "Virtual work approach to the computation of magnetic force distribution from finite element field solutions," *Proc. Inst. Elect. Eng.—Electr. Power Appl.*, vol. 147, no. 6, pp. 437–442, Nov. 2000.

[15] K. Yamazaki, S. Watari, and A. Egawa, "Adaptive finite element meshing for eddy current analysis of moving conductor," *IEEE Trans. Magn.*, vol. 40, no. 2, pp. 993–996, Mar. 2004.

Shoubao Liu was born in Hubei, China, on September 28, 1983. He received the B.S. degree in electrical engineering from the Hubei University of Technology, Wuhan, China, in 2006. He is currently working toward the Ph.D. degree in applied computational electromagnetics in the School of Electrical Engineering, Wuhan University, Wuhan.

His major fields of interest are numerical methods for electromagnetic-field calculation in engineering and electromagnetic launch.

Jiangjun Ruan was born in Zhejiang, China, on June 25, 1968. He received the B.S. and Ph.D. degrees in electric machine engineering from the Huazhong University of Science and Technology, Wuhan, China, in 1990 and 1995, respectively. He finished his postdoctoral research from the Wuhan University of Hydraulic and Electrical Engineering, Wuhan, in 1998.

He is currently a Professor with the School of Electrical Engineering, Wuhan University, Wuhan. His research interests include computational electromagnetics and high-voltage and insulation technology.

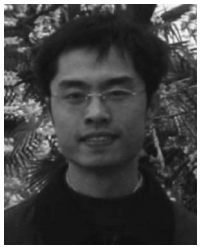

Yadong Zhang was born in Jilin, China, on October 6, 1984. He received the B.S. degree from Wuhan University, Wuhan, China, in 2006, where he is currently working toward the Ph.D. degree in the School of Electrical Engineering.

His major fields of interest are electromagnetic launch technology and its applications.

Yu Zhang was born in Jiangxi, China, on June 28, 1979. He received the B.S. degree from North China Electric Power University, Baoding, China, in 2004 and the Ph.D. degree in high-voltage and insulation technology from Wuhan University, Wuhan, China, in 2007.

He is currently with the Jiangxi Provincial Electric Power Company, Nanchang, China. His research interest is the electromagnetic environment of ultrahigh-voltage transmission lines.

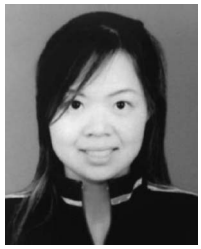

Yujiao Zhang was born in Hubei, China. She received the M.S. degree from the School of Electrical Engineering, Wuhan University, Wuhan, China, in 2005, where she is currently working toward the Ph.D. degree in electrical theory and new technology.

Her major fields of interests include numerical analysis of electromagnetic fields and multiphysics coupling and its applications in engineering.